ADVANCED THERAPEUTICS
www.advtherap.com

A Novel In Vitro Disease Model for Systemic Sclerosis Using Polyisocyanide Hydrogels

Jyoti Kumari, Tirza Wubs, Arjan P.M. van Caam, Daphne N. Dorst, Frank A. D. T. G. Wagener, and Paul H. J. Kouwer**

Systemic sclerosis (SSc) is a rare autoimmune disease with limited treatment options that is characterized by fibrosis in various organs. To screen the effectiveness of new therapies, there is an urgent need for reliable in vitro models. Key is that diseased cells' characteristics are maintained, which is challenging in currently used setups. In this study, an in vitro 3D culture system is described using the biocompatible polyisocyanide (PIC-RGD) hydrogel and SSc patient-derived fibroblasts from affected (lesional cells) and from healthy-skin (healthy cells). In contrast to the standard collagen-coated 2D cultures, the cells in the 3D PIC-RGD gels maintain the native phenotype and functionality of the primary cells. The functionality of the model is studied in the presence of the fibrosis stimulator transforming growth factor β1 (TGFβ1) and the suppressor tumor necrosis factor (TNFα). In this study, it is observed that lesional cells have a stronger fibrotic character with increased contraction, proliferation, and expression of collagen, and myofibroblast markers α-smooth muscle actin and fibroblast activation protein. The high tunability of the hydrogel, which can maintain the native functionality of fibroblasts in in vitro cultures, delivers a crucial step in developing these materials into an effective tool for personalized medicine approaches of SSc patients.

1. Introduction

Systemic sclerosis (SSc) is an autoimmune disease characterized by inflammation, vasculopathy, and severe fibrosis of connective tissues affecting first the extremities and ultimately internal organs. SSc is associated with an estimated loss of life-expectancy of more than 15 years[1] and a severely reduced quality of life.[2] The disease is rare, with an estimated incidence of 13 people per 1 million every year, but severe with high morbidities.[3] The leading cause of death is pulmonary complications that start when the disease reaches the lungs. To date, there is a lack of treatment options for SSc patients, creating a high unmet medical need.

Major contributors to the lack of treatment options are the poor understanding of SSc pathophysiology and the large disease heterogeneity, that is, it manifests differently in many patients. Consequently, there is an urgent need for personalized disease models that can examine patient-specific pathogenesis, predict disease progression, and screen for new treatment strategies and targets.[4] In vitro models are preferred over in vivo models, because they are more cost-effective, faster, and reduce the use of animals.[5] The most commonly used in vitro models are based on 2D monolayer cultures, however, they poorly resemble the in vivo disease microenvironment in terms of topography, stiffness, and viscoelasticity. Although 2D cultures are experimentally readily accessible and easily studied, they lack interconnected cell networks. Moreover, interactions between the cells and their extracellular matrix (ECM) and subsequent signaling pathways are not modeled in 2D.[6–8] To close the knowledge gap between oversimplified 2D experiments and the native tissue,[9] 3D disease models are needed that mimic the tissue microenvironment.[10] A key challenge is that the 3D models should maintain the phenotypes of different cells for example, healthy and disease-affected or lesional cells, often fibroblasts.

Recently, progress has been made to use the third dimension for in vitro SSc disease models. Collagen gels have been used as a 3D cell culture matrix,[11] which showed that collagen synthesis in lesional cells is increased compared to healthy cells. However, collagen-based gels, like other gels of biological origin, face disadvantages of poor control and batch-to-batch variations. As such, synthetic gels are more interesting since they provide a highly

J. Kumari, T. Wubs, P. H. J. Kouwer
Institute for Molecules and Materials
Radboud University
Heyendaalseweg 135, Nijmegen 6525 AJ, The Netherlands
E-mail: p.kouwer@science.ru.nl
J. Kumari, F. A. D. T. G. Wagener
Department of Dentistry – Orthodontics and Craniofacial Biology
Radboud University Medical Centre
Philips van Leydenlaan 25, Nijmegen 6525 EX, The Netherlands
E-mail: frank.wagener@radboudumc.nl
A. P. van Caam, D. N. Dorst
Department of Experimental Rheumatology
Radboudumc
Geert Grooteplein 26-28, Nijmegen 6525 GA, The Netherlands

The ORCID identification number(s) for the author(s) of this article can be found under https://doi.org/10.1002/adtp.202200180

DOI: 10.1002/adtp.202200180

reproducible cell environment.[11] Polyacrylamide-based hydrogels with varying stiffness have been used to culture healthy and SSc-derived human dermal fibroblasts.[5,12] The studied stiffness regime was, however, relatively high compared to native ECM and the cells were seeded on top of the gel instead of inside the gel. As such, the hydrogel was not used to maintain cell function but rather to study the effect of substrate stiffness on the cell behavior. Another group used a composite hydrogel of polyethylene glycol, combined with carboxymethyl chitosan, to culture mesenchymal stem cells in order to study SSc treatment.[13] Beyond these experiments, a direct comparison between healthy and SSc-derived fibroblasts is rare.

Our group developed a synthetic temperature-sensitive polyisocyanide (PIC) hydrogel that closely resembles the fibrous, porous architecture and mechanical properties of structural ECM proteins, such as collagen and fibrin.[14,15] The mechanical properties of the gel are readily modified by changing the polymer concentration (like any hydrogel) and molecular weight,[16] but, more importantly, also by external stimuli such as temperature[17] and magnetic fields[18,19] that exploit the strain-stiffing character of the material. Once decorated with cell-adhesive peptides, such as the commonly used arginine-glycine-aspartic acid motive (abbreviated RGD), the gel turns into a versatile and signal-lean 3D cell culture platform for a wide variety of cells, including stem cells,[20–21] fibroblasts,[22] kidney cells,[23] and many others,[24–30] as well as organoids.[31–33] Additionally, initial studies also show potential for PIC gels for in vivo[34,35] applications. Over the past years, PIC gels matured as a matrix that is highly tailorable in physical and biochemical properties, which is potentially advantageous when developing a simple screening approach for SSc models or, in fact, any other disease model that is characterized by a large heterogeneity.

Here, we use RGD-decorated PIC (PIC-RGD) to culture primary fibroblasts retrieved from SSc patients from lesional and disease unaffected areas. In our 3D in vitro model, we focus on maintaining the native cell functionality of both fibroblast strains. For benchmarking, we compare our results to those from a collagen-coated 2D model, which is a preferred substrate as untreated tissue culture plastic strongly affects cell behavior.[11] The efficacy of the model was studied by treating it with different soluble biological cues: stimulation (transforming growth factor β1, TGFβ1) and suppression (tumor necrosis factor, TNFα) toward developing fibrotic phenotypes, respectively. The functionality of these cells was characterized by determining the expression of alpha smooth muscle actin (αSMA), fibroblasts activation protein (FAP), and collagen 1 (COL1) as well as, at a more macroscopic scale, measuring contractile properties of both the lesional and disease unaffected cells in the PIC-RGD hydrogel.

2. Experimental Section

2.1. Synthesis of PIC-RGD Hydrogel

PIC hydrogel was synthesized as reported earlier in two steps.[20] First, azide-decorated PIC was made using the commercially available isocyanide monomer isocyano-(*D*)-alanyl-(*L*)-alanine-tri(ethylene glycol) and the corresponding azide-appended monomer (prepared in our lab) in the presence of a $Ni(ClO_4)_2 \cdot 6H_2O$ catalyst. The ratio of isocyanide monomer: azide monomer was 30:1 (3.3%) and the total monomer:catalyst ratio was 1000:1. Monomers and catalysts were mixed together in toluene and the reaction mixture was stirred overnight at room temperature. Fourier transform infrared (FTIR) confirmed the completion of the reaction by the disappearance of isocyanide absorption at 2140 cm^{-1}. The PIC polymer was then precipitated in diisopropyl ether under vigorous stirring and isolated by centrifugation. The polymer was dissolved in dichloromethane and precipitated in diisopropyl ether two more times.

The cell-adhesive peptide H-Gly-Arg-Gly-Asp-Ser-OH (GRGDS or RGD, Bachem Germany) was conjugated to the PIC polymer using DBCO-PEG_4-NHS (Bioconjugate technologies, Scottsdale, US) spacer as described earlier.[24,33] Briefly, the peptide dissolved in borate buffer (6 mg mL^{-1}) and the spacer in dimethylsulfoxide (6 mg mL^{-1}) were stirred in a molar ratio 1:1.1 peptide:spacer at room temperature. Completion of the reaction was confirmed using mass spectrometry. The azide functionalized PIC polymer (2.5 mg mL^{-1}) was dissolved in acetonitrile and added to the DBCO-RGD mixture (ratio of azide to DBCO 1:1). After 24 h of reaction, PIC conjugated GRGDS (PIC-RGD) was precipitated in diisopropyl ether, collected by centrifugation, dried, and stored in the form of a pellet. Before use in the cell culture experiments, PIC-RGD pellets were subjected to UV sterilization (254 nm, 10 min) and dissolved in sterile PBS at a concentration of 8 mg mL^{-1} at 4 °C overnight. The dissolved polymer was stored at −20 °C to be used at the time of cell seeding.

2.2. Physical Characterization of the Hydrogel

The porosity of PIC-RGD hydrogel was visualized using confocal microscopy as described earlier.[36] DBCO-Cy3 (20 μM, 1:10, Sigma (St. Louis, MO, USA) was mixed with the PIC-RGD stock solution and incubated for 30 min at 4 °C. The mixed solution was then added to a microplate and heated to 37 °C, after which the formed gel was left to equilibrate for 1 h. The microstructure of the hydrogel was then visualized using the Leica SP8× confocal microscope. Rheological experiments were carried out using a steel parallel plate geometry (20 mm) on a rheometer (Discovery HR-1, TA instruments). On the pre-cooled (5 °C) bottom plate, the PIC-RGD solution was added and the top plate was lowered. The protocol started with a temperature ramp to 37 °C at a rate of 8 °C min^{-1} and a time sweep of 15 min. Data was recorded in the linear viscoelastic regime at 1% strain with a 1 Hz frequency.

2.3. Primary Cell Isolation

Primary skin fibroblasts were isolated as described earlier.[37] Skin biopsies of size 4 mm were taken from the unaffected part and the lesional fibrotic part of the forearm of systemic sclerosis patients; in this manuscript, the cells are named healthy and lesional cells, respectively. The study protocol was approved by the local ethics committee (study number: NL57997.091.16). All patients provided written informed consent prior to the procedure. Biopsies were then cultured in a 24 well plate in the presence of complete DMEM Glutamax medium /(Gibco,Waltham, MA, USA) containing 20% fetal calf serum (FCS), 100 mg mL^{-1}

streptomycin, 100 U mL^{-1} penicillin, and 100 mg L^{-1} pyruvate in normal culture conditions (37 °C, 5% CO_2) until spontaneous outgrowth of the fibroblasts occurred. The medium was replaced twice in a week.

2.4. Cell Culture

The primary fibroblasts were cultured in complete DMEM containing 10% FCS and 1% penicillin/streptomycin 100 mg L^{-1} pyruvate until 80–90% confluency using collagen-coated T-flasks. The flasks or the plates were coated with collagen R solution 0.2%, 1:20 in PBS (Serva electrophoresis, Heidelberg, Germany) for 1 h at room temperature. For all the experiments, the passage number was between 4 and 9. For seeding, cells were harvested using trypsin-EDTA and resuspended in medium after centrifugation. For the 3D cultures, cells were mixed with cold PIC gel (final concentration 2 mg mL^{-1}) at a final concentration of 10^6 cells mL^{-1}. A hydrogel volume of 10, 100, or 300 µL was used for uncoated μ-Slide angiogenesis dishes (Ibidi, Munich, Germany), 96 well plates or 48 well plates, respectively. The hydrogel was allowed to equilibrate at 37 °C for 45 min. After the gel had solidified, the medium with three different conditions was added: 1) without supplement (untreated), 2) with TGFβ1 (Sigma, St. Louis, MO, USA, 10 ng mL^{-1}), and 3) with TNFα (Abcam ltd, Cambridge, UK, 10 ng mL^{-1}). All experiments were performed in triplicate for each cell strain. Time points used for experiments were day 3 and day 5, for the latter the medium was changed at day 3. During the medium change and different assays processing the 3D plates were kept on a hot plate at 37 °C. For the 2D cultures, before seeding, the plates were coated with collagen R solution 0.2%, 1:20 in PBS (Serva electrophoresis, Heidelberg, Germany) for 1 h at room temperature. Cells were seeded at a density of 10^4 cells mL^{-1}. The same concentration for the stimulants was used as in the 3D cultures.

2.5. Cell Spreading 3D and 2D Culture

To determine the cell spreading and physiology of the lesional and healthy cell strains in both 3D and 2D cultures, a phalloidin staining was performed. The cells were fixed with 10% formalin for 10 min on day 3 or 5. After fixation, the cells were incubated with Triton X (0.5% in PBS) for 20 min. A phalloidin solution (400× stock solution, 1:400, Molecular Probes Life technologies) was added to the cells for 1 h, followed by washing with 0.05% Tween-20/PBS and counterstaining with 4',6-diamidino-2-phenylindole (DAPI, 1 mg mL^{-1}, 1:100, Sigma, St. Louis, MO, USA) for 15 min. Finally, the cells were quickly rinsed with PBS and imaged under the SP8× AOBS-WLL confocal microscope (Leica Microsystems, Mannheim, Germany). The laser was set at a wavelength of 591 nm and UV-light.

2.6. Contraction Assay of Fibroblasts in PIC-RGD Hydrogel

The contraction of the gel was determined at day 3 and 5 in a μ-Slide. The bright field images of the hydrogel were taken at 2.5× objective and the images were analyzed using Image J software version 1.51 (NIH, MD, USA). The percentage of contraction was determined by Equation (1):

$$\text{contraction} = \frac{(A_0 - A_h)}{A_0} \times 100\% \quad (1)$$

where A_0 is the area of the plate and A_h is the area occupied by the hydrogel at day 3 or 5.

2.7. Live-Dead Assay

A live-dead staining was performed to determine if the cells remained viable after 5 days of culturing in both the 2D and 3D experiments. A solution of Calcein (2 mM; Invitrogen, Waltham, USA) and TOTO-3 (1 mM; Invitrogen, Waltham, USA) at a concentration of 1:1000 were prepared in medium and added to cells in both 3D and 2D culture for 1 h. After the incubation, the medium was removed and PBS was added. The cells were imaged under the SP8× AOBS-WLL confocal microscope (Leica Microsystems, Mannheim, Germany). The laser was set at a wavelength of 488 nm and 647 nm for Calcein and TOTO-3, respectively.

2.8. Quantifluor DNA Assay

QuantiFluor dsDNA assay kit (Promega, Madison, USA) was used to analyze the DNA concentration in a 96 well plate. The culture medium was removed from the plate and the cells were washed with PBS followed by addition of 500 µL of deionized water (MilliQ, MQ). After mixing the cell lysates were stored at −20 °C. In case of 3D culture, before adding MQ the plate was placed on ice for 20 min to make the hydrogel liquid. The quantification was subsequently performed according to the manufacturer's instruction. Briefly, quantifluor dye was prepared (1:200) in 1×TE buffer. The diluted sample (50 µL) was then mixed with dye (50 µL) and added to 96 well plate (flat bottom, black) and incubated at room temperature for 5 min in dark. The fluorescence was measured using a UV–vis spectrometry (Tecan Spark M10 plate reader) ($\lambda_{excitation}$ = 485 nm, $\lambda_{emission}$ = 530 nm). The fluorescence was normalized with day 0 value.

2.9. Viability Assay CCK8

The proliferation and cell viability of the lesional and healthy cell strains were performed using a Cell Counting Kit-8 (CCK8; Sigma,St. Louis, MO, USA) according to manufacturer's instructions in a 96 well plate. Briefly, in both 2D and 3D culture the medium was removed from the wells followed by a PBS wash. CCK8 solution (1:10) was prepared in plain medium (DMEM GlutaMAX) and added to the cells followed by incubation for 2 h at 37 °C. After incubation, the absorbance was measured at 460 nm using a Tecan Spark M10 plate reader (Tecan Group Ltd., Männedorf, Switzerland). The absorbance was normalized with the day 0 value.

2.10. Immunostaining

Immunostaining was done for αSMA, FAP, and COL-1 in micro plates. The cells were fixed with 10% formalin for 10 min, and permeabilized with TritonX-100 (0.5% in phosphate-buffered saline, PBS) for 20 min. After washing, the cells were incubated in a blocking buffer (2% w/v bovine serum albumin, BSA, 2% normal donkey serum, 0.05% Tween-20, 0.025% v/v Triton-X) with 100 mM glycine for 30 min. The primary antibodies, mouse anti human αSMA (1:800, Sigma (St. Louis, MO, USA) or rabbit anti human FAP (1:250, LN031634, LabNed, The Netherlands) or rabbit anti human COL-1 (1:200, Cedarlane labs (Burlington, Canada)) were added separately to the plate and placed in incubator overnight at 37 °C (3D) or 4 °C (2D).The next day, after washing with Tween-20, secondary antibodies (αSMA: Gt-aMo-Af594 (1:200); FAP and COL-1: Gt-aRb-Af488 (1:200)) were added for 1 h followed by washing with Tween-20 and counterstaining with DAPI (1 mg mL^{-1}, 1:100) for 15 min. The cells were quickly rinsed with PBS and imaged under the SP8x AOBS-WLL confocal microscope using 405, Alexa fluor 594 and 488 (Leica Microsystems, Mannheim, Germany).

2.11. Total Collagen Production

To analyze total collagen production, both the lesional and healthy cells were cultured in the presence of ascorbic acid (170 μM, Sigma Sigma, St. Louis, MO, USA) in 3D culture on a μ-Slide. The cells were fixed with 10% formalin for 10 min. CNA-OG488 collagen dye (Department of Biomedical engineering, TU/e Eindhoven, The Netherlands) solution (1:50 in PBS) was added to the fixed cells, and incubated overnight at 37 °C. After incubation the cells were washed with PBS and incubated with DAPI (1 mg mL^{-1}, 1:100) for 15 min. The cells were quickly rinsed with PBS and imaged under the SP8× AOBS-WLL confocal microscope (Leica Microsystems, Mannheim, Germany). The laser was set at a wavelength of 488 nm for CNA and UV-light for DAPI.

2.12. RT-qPCR

Gene expression was analyzed using RT-qPCR. The cells were extracted using different 3D and 2D study protocols. For the 3D cultures, the hydrogels were washed with warm PBS after removing the excess medium. Then, cold PBS was added to hydrogel for 5 mins and the solutions were collected by centrifugation at 400 × *g* for 5 min at 4 °C. Cold PBS facilitates the liquification of the hydrogel and provides easy isolation of the cell pellet. For the 2D cultures, after removing the culture medium and washing, the cells were harvested with TE followed by centrifuge at 400 × *g* for 5 min at 4 °C. The collected cell pellet was then used to isolate total RNA using RNeasy Micro Kit (Qiagen) according to the manufacturer's instructions. cDNA was made from the RNA using the iSCRIPT cDNA synthesis kit (BIO RAD, CA, USA). RT-qPCR was performed using SYBR green supermix (BIO RAD) with forward and reverse primers for *GAPDH*, *ACTA2*, *FAP*, and *COL1A1* (**Table 1**). The reaction conditions used were 3 min at 95 °C, followed by 39 cycles of 95 °C for 15 s and 60 °C for 30 s.

Table 1. Primer sequences for real time PCR.

Gene	Forward primer	Reverse primer
GAPDH	ATCTTCTTTTGCGTCGCCAG	TTCCCCATGGTGTCTGAGC
ACTA2	CTGACCCTGAAGTACCCGATA	GAGTGGTGCCAGATCTTTTCC
FAP	GCTTTGAAAAATATCCAGCTGCC	ACCACCATACACTTGAATTAGCA
COL1A1	AGATCGAGAACATCCGGAG	AGTACTCTCCACTCTTCCAG

The average C_t value of the experimental control and reference (GAPDH) genes were used to calculate ΔC_t and $\Delta\Delta C_t$ using the following equations:

$$\Delta C_t = C_t\left(\text{targetgene}\right) - C_t\left(\text{referencegene}\right) \quad (2)$$

$$\Delta\Delta C_t = \Delta C_t\,(\text{experimental}) - \Delta C_t\,(\text{control}) \quad (3)$$

The gene expression is represented in terms of fold change (= $2^{-\Delta\Delta Ct}$).

2.13. Image Analysis

Image J was used to analyze all the images as described earlier.[38] Briefly, area, mean gray value and integrated density were calculated randomly in different area of interest as well as for background regions (areas with no fluorescence). Furthermore, in the area of interest the total number of cells was counted to normalize the fluorescence intensities. Data represented as CTCF normalized with total cell number. The intensities were quantified using Equation (4):

$$\text{CTCF} = \text{IntDen} - (\text{area} \times \text{mean}) \quad (4)$$

where CTCF is the corrected total cell fluorescence, IntDen is the Integrated density, area is the area of selected cell and mean is the mean fluorescence of background readings.

2.14. Statistical Analysis

All data is presented as mean ± standard deviation. The significance differences were assessed between the mean values of two groups using student *t*-test or one-way analysis of variance (ANOVA) between multiple groups, where $p < 0.05$ was considered statistically significant. Type of statics test, sample sizes, and significance are given in the captions of the figures.

3. Results and Discussion

3.1. 3D PIC-RGD Hydrogel Physical Properties

For our studies, we used the adhesive peptide-decorated polymer PIC-RGD (**Figure 1**A). The synthesis is a two-step process: first an azide decorated PIC polymer is prepared by copolymerization. Secondly, a post-modification step introduces a cyclooctyne-modified peptide using the highly efficient strain-promoted

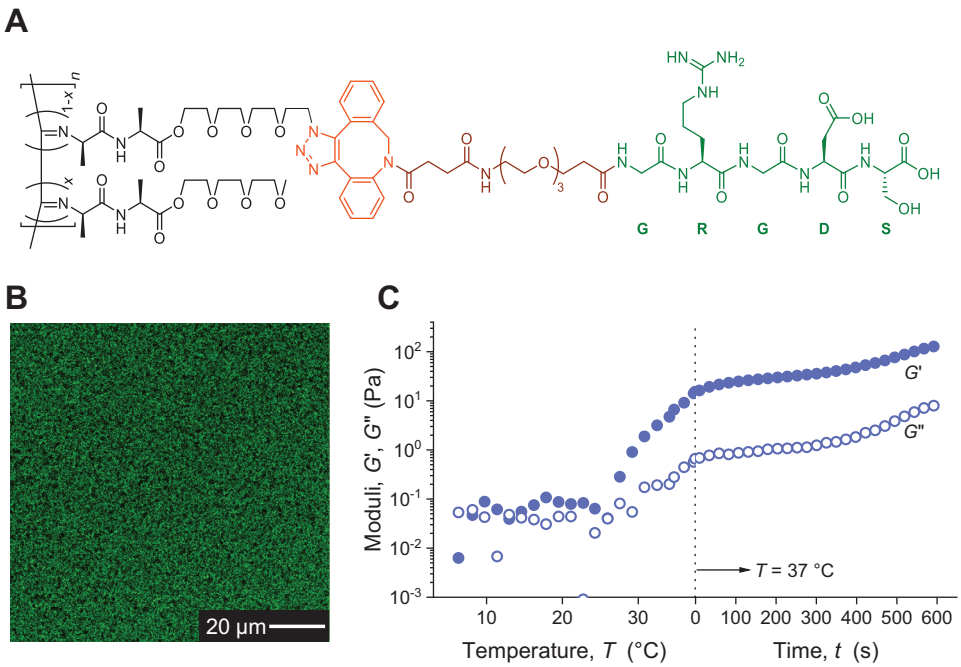

Figure 1. PIC-RGD structure and physical properties. A) Molecular structure of PIC-RGD, B) confocal fluorescence image of Cy3-labeled PIC-RGD gel (2 mg mL^{-1} in deionized water). Scale bar is 20 μm; C) Storage modulus G' and loss modulus G'' of PIC-RGD hydrogel. Left panel: heating ramp show gelation starts at ≈25 °C, after 10 min of equilibration, a soft gel with $G' \approx 100$ Pa is formed.

azide-alkyne cycloaddition (SPAAC) reaction.[20,39] The synthesis is described in detail before[40] and summarized in Figure S1, Supporting Information. An aqueous PIC-RGD solution is temperature-sensitive; it is a low viscous liquid at 4 °C and forms an elastic hydrogel at 37 °C. For this study, we have used a polymer concentration of 2 mg mL^{-1}, which is based on our earlier work where we showed that these gels recapitulate the natural environment of fibroblasts well.[22] At this concentration, we can easily discriminate between fibroblasts and myofibroblasts as the more robust contractile properties of the latter induces a strong macroscopic contraction of the gel.

During gelation the polymer forms an interconnected network of fibers that yields a heterogenous fibrous and porous architecture.[36] The network structure was visualized by conjugating a cyclooctyne-equipped fluorescent dye (DBCO-Cy3) to the hydrogel using the same SPAAC reaction, and mapping taking confocal fluorescence microscopy images (Figure 1B). Previously, our group determined the pore size of PIC gels with lower concentrations (0.25–1 mg mL^{-1}) from fluorescence measurements and subsequent quantitative analysis and found that average pore sizes varied in the micrometer range.[36] We also found that, as the concentration increases further the pore size will decrease and, as a result, we did not measure pore sizes during the cell culture experiments.

The mechanical properties of the hydrogel were evaluated by oscillatory shear rheology experiments (Figure 1C). The result shows that hydrogel gelation is thermally induced. At 37 °C, the hydrogel is soft and elastic in nature when storage modulus $G' = 91$ Pa is much larger than the loss modulus G''. As expected for a mostly elastic hydrogel, both G' and G'' were constant in the frequency range from 0.1 to 10 Hz (Figure S2, Supporting Information). These results are in line with the previous studies on PIC hydrogels.[16]

3.2. Fibroblasts form Interconnected Networks in 3D PIC-RGD Gels

For cell culture experiments, fibroblasts from healthy tissue and from affected tissue (lesional cells) of SSc patients were dispersed in a cold PIC solution in the appropriate medium, pipetted in the well and the plate was placed in an incubator at 37 °C (where gelation occurs within a minute). As a control, cells were cultured in 2D on collagen-coated tissue culture plastic. All cell cultures were studied on day 3 and 5 after seeding.

F-actin staining (phalloidin, **Figure 2**A and Figure S3A, Supporting Information) clearly shows a spread-out morphology of the fibroblasts, both in the 2D and the 3D experiments. In 3D, the PIG-RGD hydrogel allows both lesional and healthy cells to form a 3D interconnected network in an in vitro cell construct. The F-actin density was quantified by calculating the CTCF (Figure 2B and Figure S3B, Supporting Information) normalized to the cell density, obtained by nuclear staining (DAPI). The analysis shows a significant difference between healthy and lesional cells, where the latter show more spreading. The addition of TGFβ1 further enhanced cell spreading in both groups compared to the untreated samples (at day 5: lesional 1.7- fold; healthy 1.5-fold). Conversely, spreading of the cells incubated with TNFα is similar to the untreated group. In the 2D cultures, we find no significant differences between lesional and healthy fibroblasts in the untreated or in the TGFβ1 of TNFα treated cells. It is important to consider that the initial cell concentration is ≈100-fold

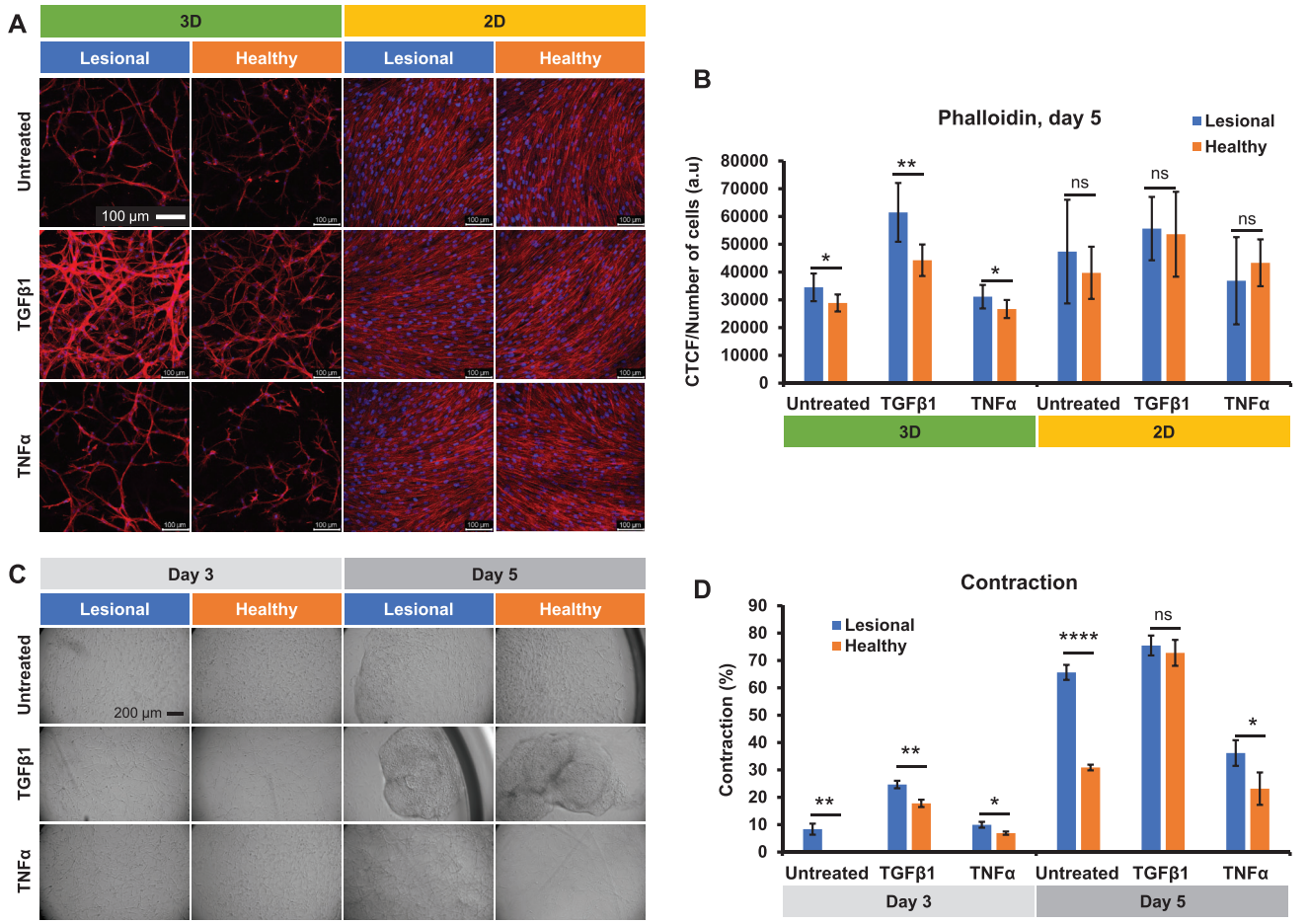

Figure 2. Cell spreading and contraction analysis. A) Confocal images showing cell spreading in 3D (left column) and 2D cultures (right column) in untreated, TGFβ1 and TNFα incubated groups of both lesional and healthy cells; B) quantitative analysis of confocal images: the corrected total cell fluorescence (CTCF) of the phalloidin channel normalized to the cell number in the DAPI channel; number of images: $n = 8$; C) Brightfield images showing contraction in PIC-RGD hydrogel encapsulated with lesional and healthy cells at day 3 (left column) and day 5 (right column) in all groups; D) quantitative image analysis of bright field images showing extent of contraction (in% of the sample at seeding) of the PIC-RGD hydrogel at day 3 and day 5; $n = 3$. Scale bar (panels (A) and (C)): 100 µm. Statistical analysis: unpaired *t*-test; *p*-values > 0.05 are not significant; significant differences: *, $p \leq 0.05$; **, $p \leq 0.01$; ***, $p \leq 0.001$, ****, $p \leq 0.0001$.

lower in 2D experiments compared to the 3D cultures. The cells seeded on the collagen-coated plate were mostly on top of each other, crowded, flat, and stretched, whereas in 3D culture cells were spread in a large surface area. This makes it difficult to identify differences between different 2D cell cultures after extended incubation times.[10]

3.3. Macroscopic Contraction of 3D PIC-RGD Gels as a Tool to Study Fibroblast Activation

Scar tissue is rich in myofibroblasts, which play a leading role in wound contraction. As a functional assay, we analyzed the contraction of lesional and healthy cells in our 3D hydrogel, an assay that is not possible for 2D cultures. Figure 2C shows the contraction of the cell cultures of the healthy and lesional cells, untreated as well as TGFβ1 and TNFα treated. Quantification (Figure 2D) shows that healthy fibroblasts contract less than lesional cells on day 3: 0% versus 8%, day 5: 31 vs 65%), which is most prominent on day 5. The higher contractility of lesional cells indicates their fibrotic nature compared to healthy, non-stimulated fibroblasts.[41] The PIC-RGD hydrogel is able to maintain the (absence of) fibrotic properties of both cell strains in vitro.

With the distinct difference in contraction between the two fibroblast strains, we anticipated that treatment of the cultures with TGFβ1 would increase the contraction of the healthy cells much stronger than the already activated lesional cells. Indeed, the effect of TGFβ1 is particularly evident on day 5 where both cultures of healthy and lesional cells contracted ≈75%. These findings are in line with other studies that demonstrated that the addition of TGFβ1 enhances the contraction of myofibroblasts and simultaneously converts quiescent fibroblasts to activated (myo)fibroblasts. [42] In contrast, upon TNFα addition contraction was reduced, most significant for the lesional cells. After 5 days in culture, the differences between the two cell strains are much smaller than in the non-treated group. Again, our results fit

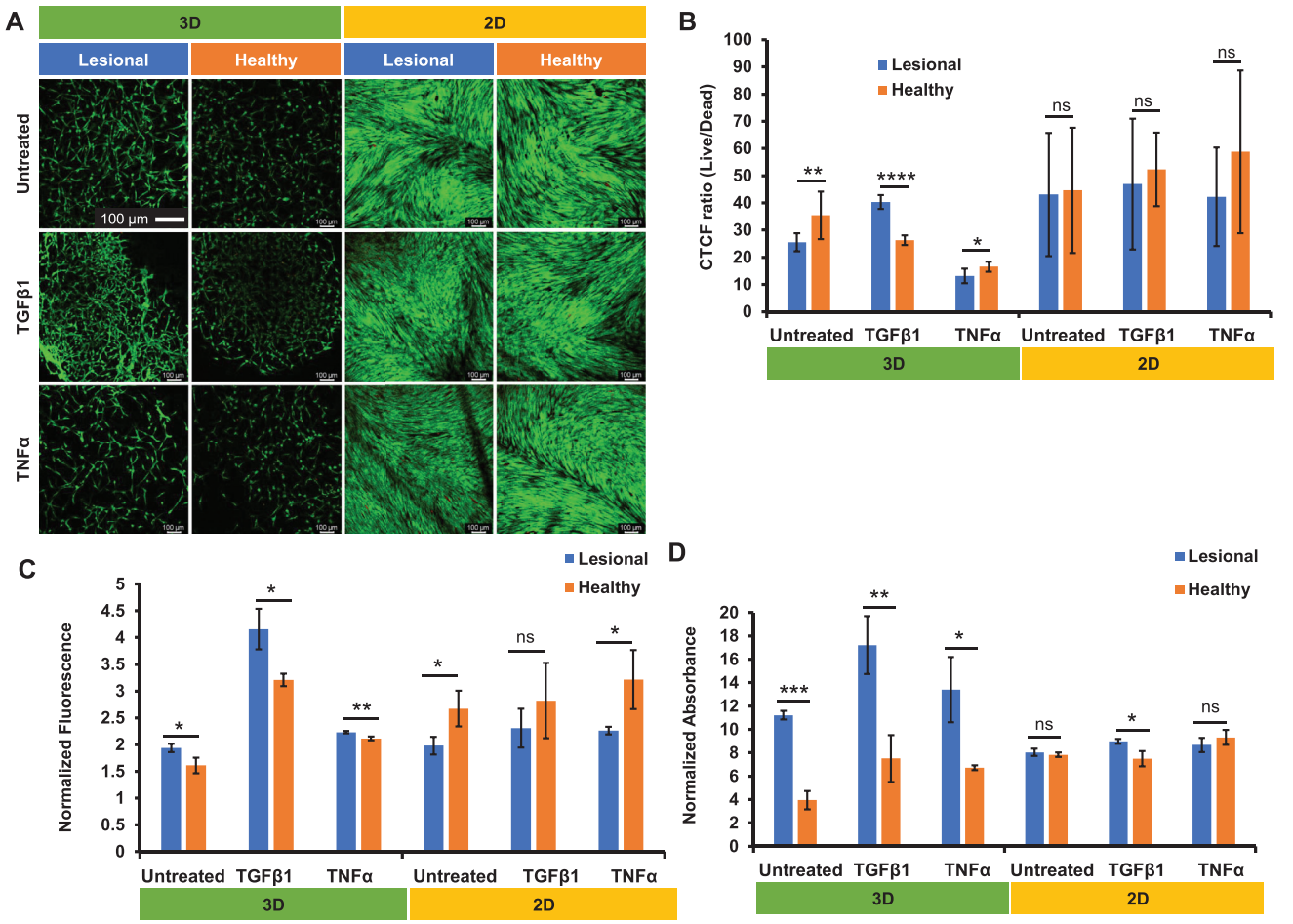

Figure 3. Cell viability and proliferation results in 3D and 2D cultures. A) Confocal images showing alive and dead cells at day 5. Living cells (green) and dead cells (red) were stained with Calcein-AM and TOTO-3, respectively; B) quantitative analysis of the confocal images of live and dead cells, expressed as the fluorescence intensity ratio Live/Dead, $n = 8$. C) Mitochondrial activity (CCK8) assay results for cell viability at day 5, $n = 3$; D) Total DNA quantification assay (QuantiFluor) results at day 5, $n = 3$. Scale bar (panel A): 100 µm. Statistical analysis: unpaired t-test; P-values > 0.05 are not significant; significant differences: *, $p \leq 0.05$; **, $p \leq 0.01$; ***, $p \leq 0.001$, ****, $p \leq 0.0001$.

earlier findings that indicate that TNFα inhibits the contraction of myofibroblasts.[43] As the 3D hydrogel showed more contraction and a more interconnected network on day 5 than on day 3, we focused in other experiments more on the day 5 cell culture results.

3.4. Biocompatibility of Fibroblasts in 3D PIC-RGD Gels and 2D Culture

Cell survival, proliferation, and mitochondrial function in 3D matrix and 2D experiments are crucial characteristics for in vitro assays.[44] Here, we performed a Live–Dead assay, a total DNA quantification assay and a mitochondrial activity assay and to assess the applicability of the material as a suitable matrix and to compare the results from the 3D studies compare to those from the previous 2D work. The Live–Dead assay was carried out for both the 3D and 2D cultures at day 5. Live cells stain green (calcein-AM) and dead cells stain red (TOTO-3). The results (**Figure 3**A) show that in all cultures, 2D and 3D, the cells were highly viable and only a few cells were dead. Quantification by taking the ratio of the green and red CTCF channels (Figure 3B) shows that differences between lesional and healthy fibroblasts are small and that viability was not impacted much by TGFβ1 or TNFα treatment. Further, image analysis showed a decrease in live cell ratio of lesional cells compared to healthy cells in untreated and TNFα 3D groups. Moreover, quantitative DNA analysis confirmed the results.

The number of cells was assessed quantitatively by determining total DNA levels through a QuantiFluor assay. For the 3D cultures, higher numbers of lesional fibroblasts were observed than healthy fibroblasts, which was more pronounced at day 5 (Figure 3C) than at day 3 (Figure S4A, Supporting Information). Furthermore, we observed only limited significant differences for the 2D cultures. The DNA assay results show that the lesional cells are proliferating more than healthy cells in our 3D culture. This result fits with previous studies that showed that myofibroblasts grow faster than quiescent fibroblasts.[41]

The mitochondrial activity of the cells was measured through a CCK8 assay. The CCK8 results were represented as absorbances normalized to the values at day 0. For the 3D cultures, as expected we observed a significantly stronger mitochondrial activity of the lesional cells compared to the healthy cells at day 3 (Figure S4B, Supporting Information) and at day 5 (Figure 3D). Interestingly, the results were in line with proliferation assay but contradict the live-dead assay in case of 3D untreated and TNFα group. Normally more viability means a greater number of living cells, which corresponds to more mitochondrial activity. But here, we did not find this correlation between live cell image analysis and CCK8 assay results. One may rationalize the discrepancy by an increased number of mitochondria per cell. TGFβ-induced myofibroblast formation results in mitochondrial biogenesis and glycolysis,[45] which may explain why lesional cells exert more mitochondrial activity as shown by the CCK8 assay. Note that the number of mitochondria per cell are preferentially increased in the lesional cells when grown under 3D but not under 2D conditions. Additionally, at day 5, both TGFβ1 and TNFα enhanced the proliferation (1.5 and 1.2-fold in lesional cells; 1.9 and 1.7-fold in healthy cells), although the increase was not significant for TNFα treatment of lesional cells. Our results are in line with previous findings, where myofibroblasts proliferate faster than resting fibroblasts and TGFβ1and TNFα enhanced the proliferation of myofibroblasts.[43,46] Also, it has been shown that TGFβ1 can cause cells to inhibit apoptotic pathways, increasing their survival.[47] Interestingly, in the 2D cultures, we did not observe significant differences in absorbance of lesional and healthy cells except day 5 for the TGFβ1-treated cell (1.1-fold increase in lesional cells), see Figure 3D and Figure S4B, Supporting Information. These results are consistent with the cell spreading data (Figure 2B).

3.5. PIC-RGD Hydrogels Can Discriminate between Lesional and Healthy Cells for the Expression of Functional Fibrosis Markers

The fibrotic nature of cells can be assessed by characterizing the production of proteins such as αSMA, FAP, and collagen (type I).[48–50] We stained the 2D and 3D cultures for αSMA (**Figure 4**A) and FAP (Figure 4C) and quantified the fluorescence images with CTCF (Figure 4B,D). Col-1 (Figure 4E) and total collagen (Figure 4G) were determined and quantified (Figure 4F,H) for the 3D cultures only as the collagen coating of the tissue culture plastic of the 2D cultures interferes with the analysis.

A key marker for fibrosis is αSMA. In the 3D culture, 5 days after seeding, lesional cells produced more αSMA than healthy cells for all growth conditions, which could not be confirmed in the 2D cultures. Compared to untreated groups, addition of TGFβ1 enhanced αSMA production while TNFα reduced αSMA production. Although the effect of TGFβ1 and TNFα on αSMA production is seen in both the 2D and 3D cultures, the difference in αSMA expression between lesional and healthy fibroblasts is only observed in the 3D culture, which suggests that the hydrogel is able to provide a native environment to both lesional and healthy cells.

FAP-positive fibroblasts are present in areas of ongoing tissue remodeling, including wound healing, fibrosis and in the microenvironment of solid tumors,[51] which makes FAP a good indicator of fibrosis. We hypothesize that FAP is also overexpressed in the lesional regions of SSc patients. The staining results and the quantification (Figure 4C,D) show differences in FAP expression between lesional and healthy cells for all conditions in 3D and 2D (besides the 2D TGFβ1 treated group). In 3D cultures, FAP production was increased in the presence of TGFβ1 (2.1-fold) and reduced with TNFα treatment (0.6-fold) compared to untreated group for both lesional and healthy cells. A similar effect was observed in 2D culture, where TGFβ1 treatment enhanced the FAP production for lesions (3.3-fold) and healthy (2.4-fold) cells. However, the inhibitory effect of TNFα treatment on FAP production was seen only in healthy cells (0.7-fold).

Collagen production is an important hallmark of myofibroblasts function. Among various types of collagen, COL-1 has the highest abundance and we analyzed its production by lesional and healthy cells in our 3D hydrogel (Figure 4E,F). Compared to the non-treated fibroblasts, the presence of TGFβ1 increases COL-1 production 3.0 and 1.4-fold for lesional and healthy cells, respectively. Conversely, TNFα treatment reduces COL-1 production by 0.6 and 0.7-fold, respectively. Qualitatively, we find the same trend in total collagen production, which is higher in lesional cells (Figure 4G,H and Figure S5A,B, Supporting Information). Incubation with TGFβ1 further enhanced the production by 3.2- and 2.5-fold and TNFα group reduced the production by 0.8- and 0.9-fold in lesional and healthy cells, respectively.

In short, all markers show a similar picture confirming that lesional fibroblasts of SSc patients have a stronger fibrotic character than their healthy counterparts. This difference is more pronounced in the 3D cell cultures compared to 2D culture. Moreover, for all tested fibrosis markers it was found that the addition of TGFβ1 increases and TNFα decreases production.

3.6. Differentiation between Lesional and Healthy Cells at the Gene Level of Fibrotic Markers

In addition to immunostaining we performed qRT-PCR for different fibrotic marker genes at day 5 for both cell cultures. The gene expression is represented as the fold change in expression of lesional cells with respect to healthy cells, normalized to the housekeeping gene (*GAPDH*) expression. For both the 3D cultures (**Figure 5**A) and the 2D experiments (Figure 5B), the expression of *ACTA2* and *COL1A1* is enhanced in untreated and TGFβ1-treated cells and reduced in TNFα stimulated cells. The result is in line with previous studies that found that myofibroblasts express more *ACTA2* and *COL1A1* and that expression is further enhanced by TGFβ1 and reduced by TNFα addition.[52–56] We note that differences in *ACTA2* expression for the different conditions were significant for the 3D hydrogel cultures but not for the 2D studies. In contrast, gene expression of *FAP* is not upregulated in untreated cells in both 3D and 2D cultures. Treatment with TGFβ1 and TNFα does induce some increased and decreased expression in lesional cells compared to healthy cells, parallel to the expression of *ACTA2* and *COL1A1*.

4. Conclusions

In summary, this study shows that the 3D PIC-RGD hydrogel can be used to culture lesional SSc-derived fibroblasts in vitro, which

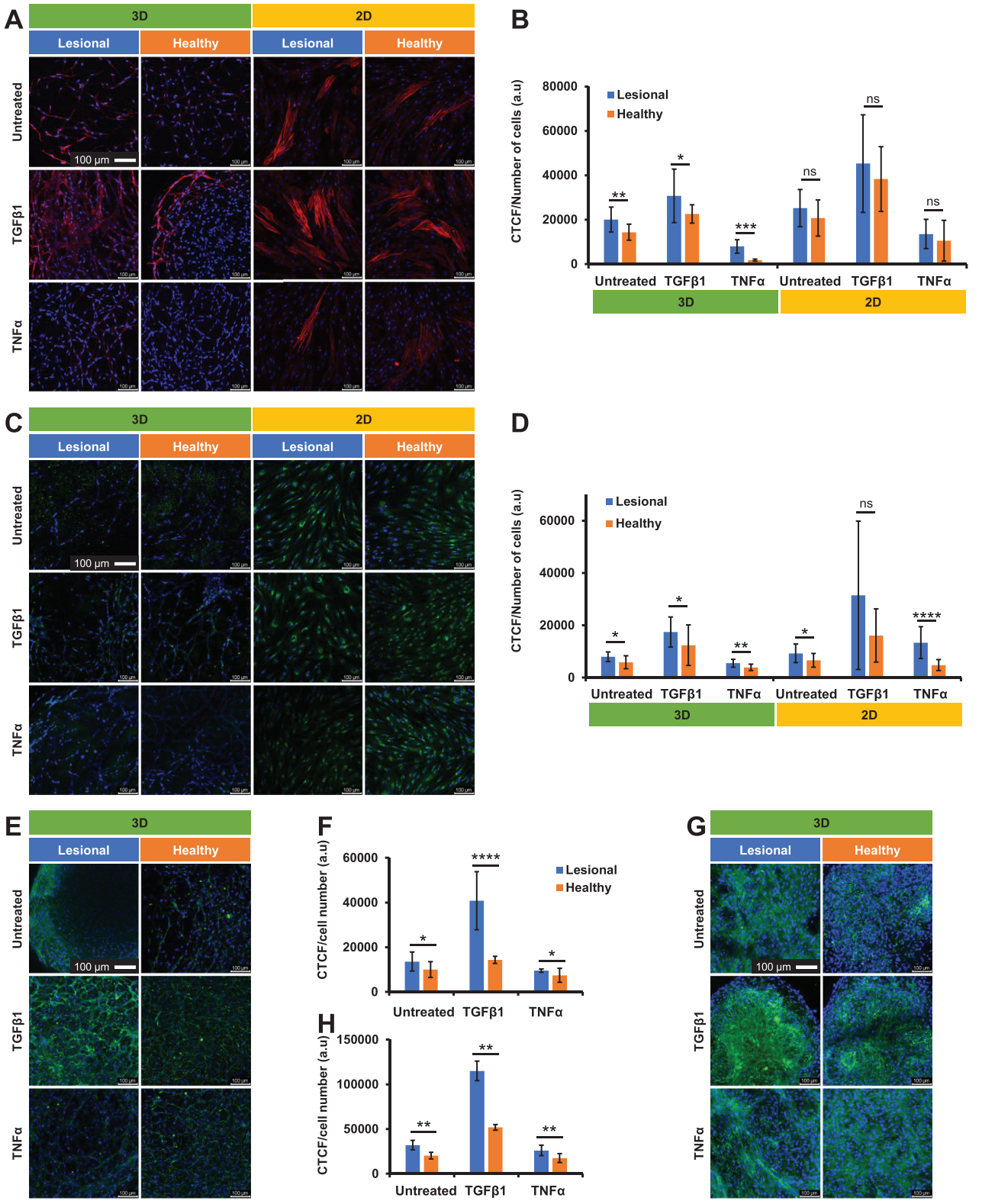

Figure 4. Immunostaining and total collagen production. A,C,E,G) Confocal fluorescence images of immunostaining of αSMA (red, A), FAP (green, C), COL-1 (green, E), and total collagen (green, G). All samples were counterstained with DAPI for the nuclei (blue). Images taken at day 5, for 3D cultures (all samples) and 2D cultures (αSMA and FAP). Scale bars: 100 µm. B,D,F,H) Quantitative image analysis of α-SMA (B), FAP (D), COL-1 (F), and total collagen (H) production, normalized to the number of cells; $n = 16$. Statistical analysis: unpaired t-test; p-values > 0.05 are not significant; significant differences: *, $p \leq 0.05$; **, $p \leq 0.01$; ***, $p \leq 0.001$, ****, $p \leq 0.0001$.

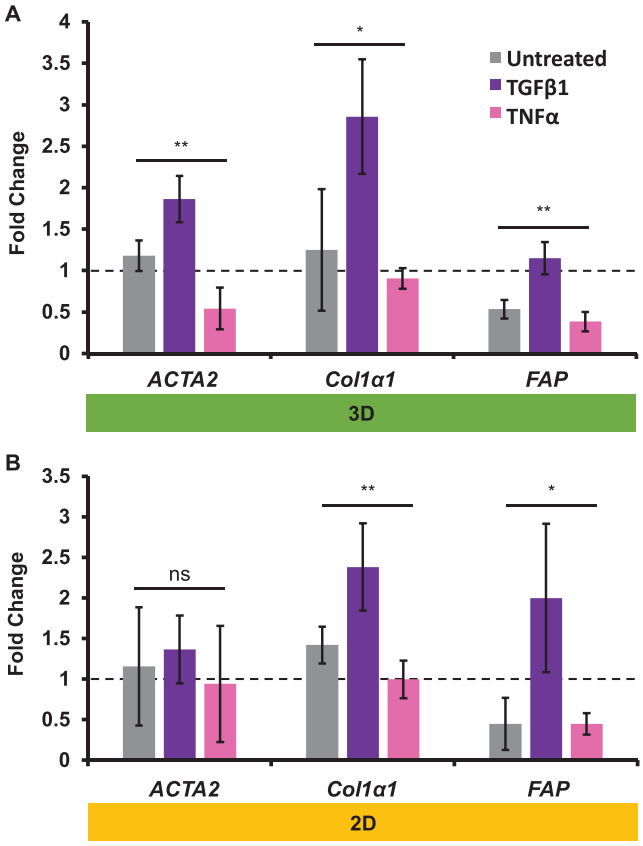

Figure 5. Gene expression analysis in 3D and 2D cultures. A,B) Increase of mRNA gene-expression of *ACTA2*, *Col1α1*, and *FAP* of lesional cells compared to healthy cells in PIC-RGD hydrogel (A) and 2D culture (B) at day 5, $n = 3$. Statistical analysis with one-way ANOVA. p-values > 0.05 are considered not significant (ns); significant differences: *, $p \leq 0.05$; **, $p \leq 0.01$.

	3D			2D		
	untreated	+ TGFβ1	+TNFα	untreated	+ TGFβ1	+TNFα
F-action production	▲	▲	▲	–	–	–
contraction	▲	▲	▲	–	–	▲
cell viability	▼	▲	▼	–	–	–
proliferation (CCK8)	▲	▲	▲	–	▲	–
αSMA production	▲	▲	▲	–	–	–
FAP production	▲	▲	▲	▲	–	▲
collagen type I	▲	▲	▲	n/a		
total collagen	▲	▲	▲	n/a		

Figure 6. Schematic overview of cell culture results for the different groups. Increased (▲) or decreased (▼) expression of lesional cells compared to healthy cells, or no observable change (–). Collagen excretion could not be determined on the collagen-coated 2D plates.

maintain their native functionality (i.e., the fibrotic nature) in comparison to healthy cells. In contrast, we find that primary cells cultured under standard 2D cell culture conditions, quickly lose their phenotype, which is in line with earlier work. To the best of our knowledge, this is the first study directed at maintaining fibroblast functionality in vitro; other hydrogel studies focused on the cells' response toward the matrix's mechanical properties. To mimic and further the understanding of SSc, it is crucial that the functionality of the SSc-affected fibroblast is maintained and clearly distinct from that of the healthy, nonaffected cells within the same patient. Furthermore, we found that the fibroblasts in the 3D PIC-RGD hydrogel respond to stimulation (TGFβ1) and inhibition (TNFα) analogously to what has been described previously in the field of SSc research.

More specifically, we observed that fibroblasts inside the PIC-RGD hydrogel form an interconnected network that ultimately displays macroscopic gel contraction, characteristics that are challenging to reproduce in 2D culture. Additionally, the hydrogel reproduces the increased growth rate of lesional cells over healthy cells better than the 2D culture, including the effects of TGFβ1 and TNFα on proliferation. The increased production of myofibroblast markers in lesional cells at protein and gene level was found to be more pronounced in 3D than 2D cultures. A schematic overview of the results in all groups (**Figure 6**) clearly indicates that the 3D cultures are much more sensitive towards induced fibrotic or nonfibrotics conditions than the 2D cultures, which also shows that in the 3D PIC-RGD culture, the lesional cells maintain their fibrotic nature much better.

The synthetic nature of PIC-RGD hydrogel makes it a particularly versatile in vitro drug testing model for the following reasons: it is i) highly reproducible; ii) well controlled; and iii) allows for tailoring of the complexity of the model by addition of growth factors or other components to form composites.[15,18] Moreover, the matrix supports easy-to-use 3D co-cultures of fibroblasts with other cells of many different disorders.[57] Furthermore, due to the reversible gelation of the matrix, one can use this 3D model for downstream cell analysis, including gene analysis of lesional and healthy cells.[22] Lastly, the model is readily expanded by introducing soluble factors implicated in different disorders. In short, the developed 3D PIC-RGD model offers an attractive route towards high-throughput drug screening and development of personalized medicine treatment strategies.

Supporting Information

Supporting Information is available from the Wiley Online Library or from the author.

Acknowledgements

The authors acknowledge funding for the research leading to these results from the Ministry of Education, Culture and Science (Gravitation program 024.001.035). Figure 6 was corrected on January 20, 2023.

Conflict of Interest

The authors declare no conflict of interest.

Data Availability Statement

The data that support the findings of this study are available from the corresponding author upon reasonable request.

Keywords

disease models, myofibroblasts, polyisocyanides, sclerosis, synthetic hydrogels

Received: August 9, 2022
Revised: November 9, 2022
Published online: December 9, 2022

[1] C. C. Mok, C. L. Kwok, L. Y. Ho, P. T. Chan, S. F. Yip, *Arthritis Rheum.* **2011**, *63*, 1182.
[2] C. Almeida, I. Almeida, C. Vasconcelos, *Autoimmun. Rev.* **2015**, *14*, 1087.
[3] A. P. v. Caam, M. C. Vonk, F. H. J. v. d. Hoogen, P. L. v. Lent, P. M. v. d. Kraan, *Front. Immunol.* **2018**, *9*, 2452.
[4] P. Khedoe, E. Marges, P. Hiemstra, M. Ninaber, M. Geelhoed, *Front. Immunol.* **2020**, *11*, 1990.
[5] A. De Pieri, B. D. Korman, A. Jungel, K. Wuertz-Kozak, *Adv. Biol.* **2021**, *5*, 2000168.
[6] C. Jensen, Y. Teng, *Front. Mol. Biosci.* **2020**, *7*, 33.
[7] K. Duval, H. Grover, L. H. Han, Y. Mou, A. F. Pegoraro, J. Fredberg, Z. Chen, *Physiology* **2017**, *32*, 266.
[8] A. S. Khalil, R. Jaenisch, D. J. Mooney, *Adv. Drug Delivery Rev.* **2020**, *158*, 116.
[9] E. R. Shamir, A. J. Ewald, *Nat. Rev. Mol. Cell Biol.* **2014**, *15*, 647.
[10] R. Edmondson, J. J. Broglie, A. F. Adcock, L. Yang, *Assay Drug Dev. Technol.* **2014**, *12*, 207.
[11] S. M. Garrett, D. Baker Frost, C. Feghali-Bostwick, *J. Scleroderma Relat. Disord.* **2017**, *2*, 69.
[12] T. Toyama, A. P. Looney, B. M. Baker, L. Stawski, P. Haines, R. Simms, A. D. Szymaniak, X. Varelas, M. Trojanowska, *J. Invest. Dermatol.* **2018**, *138*, 78.
[13] M. Nie, B. Kong, G. Chen, Y. Xie, Y. Zhao, L. Sun, *Bioact. Mater.* **2022**, *17*, 369.
[14] P. H. J. Kouwer, M. Koepf, V. A. A. Le Sage, M. Jaspers, A. M. van Buul, Z. H. Eksteen-Akeroyd, T. Woltinge, E. Schwartz, H. J. Kitto, R. Hoogenboom, S. J. Picken, R. J. M. Nolte, E. Mendes, A. E. Rowan, *Nature* **2013**, *493*, 651.
[15] K. Liu, M. Wiendels, H. Yuan, C. Ruan, P. H. J. Kouwer, *Bioact. Mater.* **2022**, *9*, 316.
[16] M. Jaspers, M. Dennison, M. F. J. Mabesoone, F. C. MacKintosh, A. E. Rowan, P. H. J. Kouwer, *Nat. Commun.* **2014**, *5*, 5808.
[17] P. de Almeida, M. Jaspers, S. Vaessen, O. Tagit, G. Portale, A. E. Rowan, P. H. J. Kouwer, *Nat. Commun.* **2019**, *10*, 609.
[18] W. Chen, Y. Zhang, J. Kumari, H. Engelkamp, P. H. J. Kouwer, *Nano Lett.* **2021**, *21*, 6740.
[19] W. Chen, J. Kumari, H. Yuan, F. Yang, P. H. J. Kouwer, *Adv. Mater.* **2022**, *34*, 2202057.
[20] K. Liu, S. M. Mihaila, A. Rowan, E. Oosterwijk, P. H. Kouwer, *Biomacromolecules* **2019**, *20*, 826.
[21] K. Liu, T. Veenendaal, M. Wiendels, A. M. Ruiz-Zapata, J. van Laar, R. Kyranas, H. Enting, B. van Cranenbroek, H. J. P. M. Koenen, S. M. Mihaila, E. Oosterwijk, P. H. J. Kouwer, *ACS Appl. Mater. Interfaces* **2020**, *12*, 56723.
[22] J. Kumari, F. A. D. T. G. Wagener, P. H. J. Kouwer, *ACS Appl. Mater. Interfaces* **2022**, *14*, 19212.
[23] Y. Zhang, M. M. P. Zegers, A. Nagelkerke, A. E. Rowan, P. N. Span, P. H. J. Kouwer, *Adv. Sci.* **2021**, *8*, 2003380.
[24] J. Zimoch, J. S. Padial, A. S. Klar, Q. Vallmajo-Martin, M. Meuli, T. Biedermann, C. J. Wilson, A. Rowan, E. Reichmann, *Acta Biomater.* **2018**, *70*, 129.
[25] R. Yegappan, J. Lauko, Z. Wang, M. F. Lavin, A. W. Kijas, A. E. Rowan, *Adv. Healthcare Mater.* **2022**, *11*, 2200574.
[26] C. Ma, K. Liu, Q. Li, Y. Xiong, C. Xu, W. Zhang, C. Ruan, X. Li, X. Lei, *Bioengineering* **2022**, *9*, 453.
[27] J. Weiden, D. Voerman, Y. Dölen, R. K. Das, A. van Duffelen, R. Hammink, L. J. Eggermont, A. E. Rowan, J. Tel, C. G. Figdor, *Front. Immunol.* **2018**, *9*, 2798.
[28] Z. Liu, J. Fu, H. Yuan, B. Ma, Z. Cao, Y. Chen, C. Xing, X. Niu, N. Li, H. Wang, H. An, *Acta Biomater.* **2022**, *148*, 152.
[29] B. M. Tiemeijer, M. W. D. Sweep, J. J. F. Sleeboom, K. J. Steps, J. F. van Sprang, P. De Almeida, R. Hammink, P. H. J. Kouwer, A. I. P. M. Smits, J. Tel, *Front. Bioeng. Biotechn.* **2021**, *9*, 715408.
[30] Z. Zhang, C. Tang, R. Hammink, F. Nelissen, H. Heus, P. H. J. Kouwer, *Chem. Commun.* **2021**, *57*, 2744.
[31] S. Ye, J. W. B. Boeter, M. Mihajlovic, F. G. van Steenbeek, M. E. van Wolferen, L. A. Oosterhoff, A. Marsee, M. Caiazzo, L. J. W. van der Laan, L. C. Penning, T. Vermonden, B. Spee, K. Schneeberger, *Adv. Funct. Mater.* **2020**, *30*, 2000893.
[32] S. Ye, J. W. B. Boeter, L. C. Penning, B. Spee, K. Schneeberger, *Bioengineering* **2019**, *6*, 59.
[33] Y. Zhang, C. Tang, P. N. Span, A. E. Rowan, T. W. Aalders, J. A. Schalken, G. J. Adema, P. H. J. Kouwer, M. M. P. Zegers, M. Ansems, *Adv. Sci.* **2020**, *7*, 2001797.
[34] R. C. op 't Veld, O. I. van den Boomen, D. M. S. Lundvig, E. M. Bronkhorst, P. H. J. Kouwer, J. A. Jansen, E. Middelkoop, J. W. Von den Hoff, A. E. Rowan, F. A. D. T. G. Wagener, *Biomaterials* **2018**, *181*, 392.
[35] B. Wang, J. Wang, J. Shao, P. H. J. Kouwer, E. M. Bronkhorst, J. A. Jansen, X. F. Walboomers, F. Yang, *J. Controlled Release* **2020**, *324*, 134.
[36] J. Vandaele, B. Louis, K. Liu, R. Camacho, P. H. J. Kouwer, S. Rocha, *Soft Matter* **2020**, *16*, 4210.
[37] D. N. Dorst, A. P. M. van Caam, E. L. Vitters, B. Walgreen, M. M. A. Helsen, C. Klein, S. Gudi, T. Wubs, J. Kumari, M. C. Vonk, P. M. van der Kraan, M. I. Koenders, *Int. J. Mol. Sci.* **2021**, *22*, 12681.
[38] R. Fu, H. Guo, S. Janga, M. Choi, W. Klinngam, M. C. Edman, S. F. Hamm-Alvarez, *Sci. Rep.* **2020**, *10*, 1455.
[39] E. Kim, H. Koo, *Chem. Sci.* **2019**, *10*, 7835.
[40] M. Koepf, H. J. Kitto, E. Schwartz, P. H. J. Kouwer, R. J. M. Nolte, A. E. Rowan, *Eur. Polym. J.* **2013**, *49*, 1510.
[41] I. A. Darby, B. Laverdet, F. Bonte, A. Desmouliere, *Clin. Cosmet. Investig. Dermatol.* **2014**, *7*, 301.
[42] A. Vallee, Y. Lecarpentier, *Cell Biosci.* **2019**, *9*, 98.
[43] S. G. Mattyasovszky, A. Hofmann, C. Brochhausen, U. Ritz, S. Kuhn, J. Wollstadter, H. Schulze-Koops, L. P. Muller, B. Watzer, P. M. Rommens, *Arthritis Res. Ther.* **2010**, *12*, R4.
[44] M. A. M. Vis, K. Ito, S. Hofmann, *Front. Bioeng. Biotechnol.* **2020**, *8*, 911.
[45] K. Bernard, N. J. Logsdon, S. Ravi, N. Xie, B. P. Persons, S. Rangarajan, J. W. Zmijewski, K. Mitra, G. Liu, V. M. Darley-Usmar, V. J. Thannickal, *J. Biol. Chem.* **2015**, *290*, 25427.
[46] F. Strutz, M. Zeisberg, A. Renziehausen, B. Raschke, V. Becker, C. van Kooten, G. Muller, *Kidney Int.* **2001**, *59*, 579.
[47] A. Jelaska, J. H. Korn, *Arthritis Rheum.* **2000**, *43*, 2230.
[48] A. V. Shinde, C. Humeres, N. G. Frangogiannis, *Biochim. Biophys. Acta, Mol. Basis Dis.* **2017**, *1863*, 298.

[49] M. H. Fan, Q. Zhu, H. H. Li, H. J. Ra, S. Majumdar, D. L. Gulick, J. A. Jerome, D. H. Madsen, M. Christofidou-Solomidou, D. W. Speicher, W. W. Bachovchin, C. Feghali-Bostwick, E. Pure, *J. Biol. Chem.* **2016**, *291*, 8070.
[50] K. R. Kleaveland, M. Velikoff, J. Yang, M. Agarwal, R. A. Rippe, B. B. Moore, K. K. Kim, *J. Immunol.* **2014**, *193*, 5229.
[51] T. Kimura, J. Monslow, A. Klampatsa, M. Leibowitz, J. Sun, M. Liousia, P. Woodruff, E. Moon, L. Todd, E. Puré, S. M. Albelda, *Am. J. Physiol. Lung Cell Mol. Physiol.* **2019**, *317*, L271.
[52] M. M. Qadri, G. D. Jay, R. S. Ostrom, L. X. Zhang, K. A. Elsaid, *Am. J. Physiol. Cell Physiol.* **2018**, *315*, C432.
[53] P. Wei, Y. Xie, P. W. Abel, Y. Huang, Q. Ma, L. Li, J. Hao, D. W. Wolff, T. Wei, Y. Tu, *Cell Death Dis.* **2019**, *10*, 670.
[54] V. Yeung, S. Sriram, J. A. Tran, X. Guo, A. E. K. Hutcheon, J. D. Zieske, D. Karamichos, J. B. Ciolino, *Biomolecules* **2021**, *11*, 1682.
[55] M. T. Goldberg, Y. P. Han, C. Yan, M. C. Shaw, W. L. Garner, *J. Invest. Dermatol.* **2007**, *127*, 2645.
[56] A. Desmouliere, A. Geinoz, F. Gabbiani, G. Gabbiani, *J. Cell Biol.* **1993**, *122*, 103.
[57] Z. Zhang, W. Chen, D. M. Tiemessen, E. Oosterwijk, P. H. J. Kouwer, *Adv. Healthcare Mater.* **2022**, *11*, 2102389.